Int J Earth Sci (Geol Rundsch) (2010) 99:687–701
DOI 10.1007/s00531-008-0410-4

ORIGINAL PAPER

Complete recycling of a magmatic arc: evidence from chemical and isotopic composition of Quaternary trench sediments in Chile (36°–40°S)

Friedrich Lucassen · Michael Wiedicke · Gerhard Franz

Received: 16 June 2008 / Accepted: 15 December 2008 / Published online: 10 January 2009
© Springer-Verlag 2009

Abstract Marine Quaternary trench and slope sediments were sampled along the margin of the Southern Andes, Chile between 36° and 40°S. Major and trace element contents indicate only minor influence of weathering and transport fractionation. The whole rock composition of the sediments is similar to the average rock of the Cretaceous to Holocene magmatic arc of this section of the southern volcanic zone. Sr, Nd, and Pb isotope composition of the sediments also resembles closely the average composition of the magmatic arc. The contribution of compositionally distinct Palaeozoic crust, which makes up most of the volume of the forearc, is ~0–20% crustal Sr, Nd, and Pb according to the isotope record of the trench and slope sediments. Input of sediments from the continent into the subduction system was dominated by detritus from the magmatic arc at least for the last 20 My on the basis of the Oligocene to Holocene exhumation history of the margin.

Keywords Active continental margin · Trench sediments · Chemical composition · Isotope signature · Southern Andes

F. Lucassen (✉)
GeoForschungsZentrum Potsdam, Telegrafenberg, 14473 Potsdam, Germany
e-mail: lucassen@gfz-potsdam.de

F. Lucassen · G. Franz
Technische Universität Berlin, Fachgebiet Petrologie, ACK 9 Ackerstr. 71–76, 13355 Berlin, Germany

M. Wiedicke
Bundesanstalt für Geowissenschaften und Rohstoffe, Stilleweg 2, 30655 Hannover, Germany

Introduction

The sedimentary infill of the deep sea trench from the continent affects the make-up of the interface between the oceanic and the continental plate in terms of sediment accretion versus erosion, and has a large effect on the subduction channel kinematics (e.g. Shreve and Cloos 1986; Lohrmann et al. 2006). It is also a major source for input of upper crustal material to the mantle source of arc magmas (e.g. Plank and Langmuir 1998; Sigmarsson et al. 2002). The deep sea trench of the Chilean subduction zone of the segment between the subducting Chile Triple Junction at ~45°S and Juan Fernández ridge at ~33°S (Fig. 1a), which both form morphological highs, deepens from ~3,800 m below sea level at 44°S to ~5,000 m at 36°S (e.g. Lindquist et al. 2004; Kukowski and Oncken 2006). The present average trench fill is ~2 km thick with high average sedimentation rates since the Pliocene linked to glaciation/deglaciation and fast denudation of the Andean Cordillera (e.g. Melnick and Echtler 2006; Glodny et al. 2008); south of 38°S the structural trench is filled by sediments (Thornburg and Kulm 1987; Völker et al. 2006). Accumulation of these sediments in an accretionary wedge appears to be minor and subduction of sediments is considered as important (e.g. Behrmann and Kopf 2001; Kukowski and Oncken 2006). The present sediment supply from the shelf (marine forearc basins) and upper slope into the trench is largely controlled by submarine cañon linked to the major E–W drainages (rivers) of the western flank of the Andes (e.g. Thornburg and Kulm 1987; Völker et al. 2006; Fig. 1). Erosion and sedimentation occur in a geographically well-defined system. The watershed of the Andean mountains limits the source area. The sediment transport follows the E–W morphological gradient to the final depositional area, the trench. The morphological

barriers of the Chile Triple Junction and the Fernández ridge limit possible lateral sediment transfer within the trench and the depth gradient determines the general direction of sediment transport from South to North.

Geochemical studies including the isotope composition of the trench sediments are limited to the sample material of ODP Leg 141 (~45°S; Fig. 1a, Kilian and Behrmann 2003), whereas other studies address on sedimentological and petrographical aspects (Thornburg and Kulm 1987; Völker et al. 2006). This study focuses on the chemical and Nd, Sr, and Pb isotope compositions of 21 sediment samples from the trench and western slope (ts-sediments in the following) between 40° and 36°S from three sample sites related to the major sediment feeders CalleCalle, Tolten, and BioBio Cañón (Fig. 1). Our aim is to define the contribution of distinct continental sources to the ts-sediments and to characterize the composition of the influx from the continent into the subduction system.

Geology and composition of the source area

Considering the present morphology of the Chilean part of the Southern Andes, all continental sediments brought into

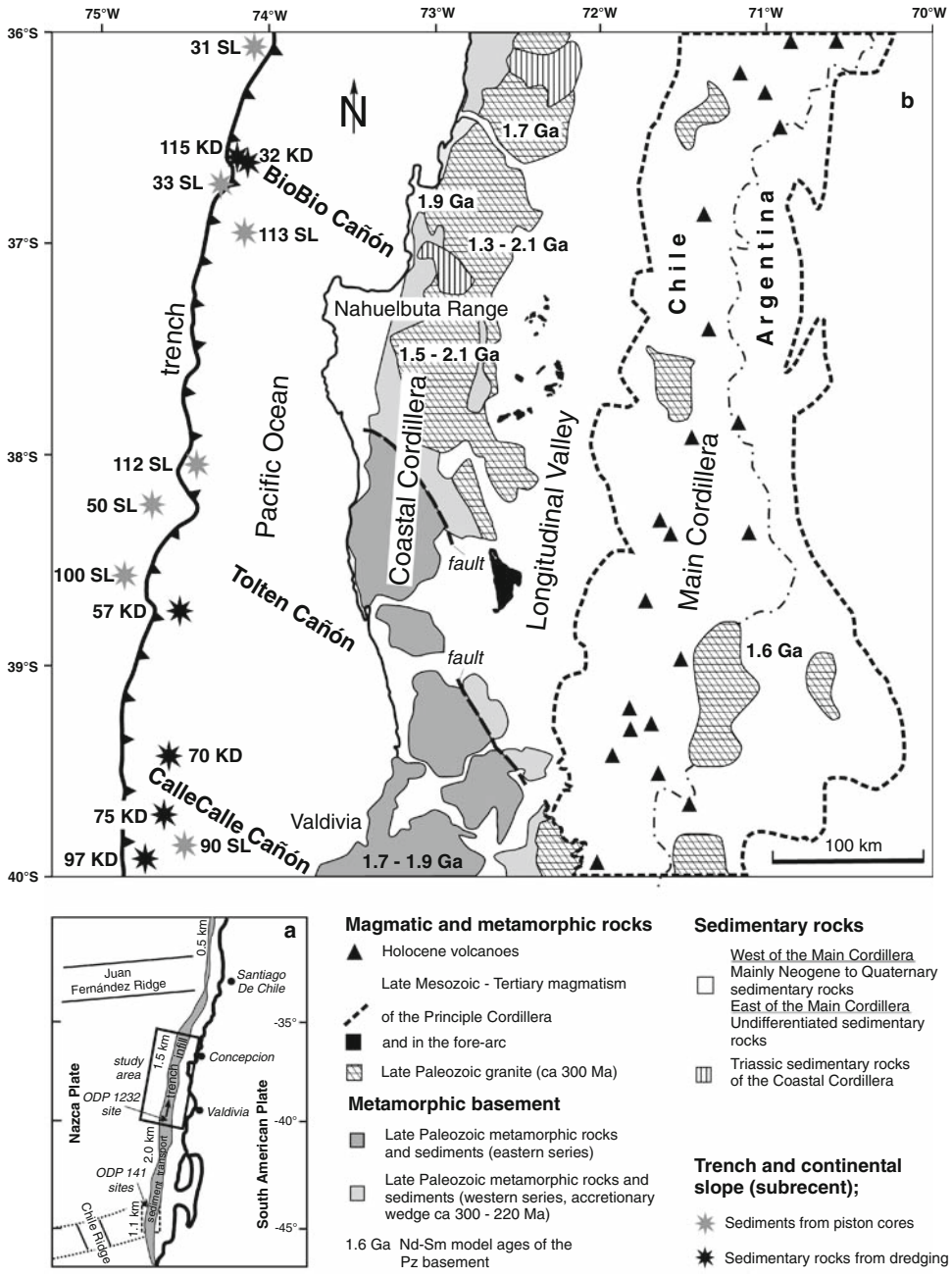

Fig. 1 Overview, geological map and sample sites of trench and slope sediments. **a** The overview shows the position of the Chile and Juan Fernández Ridge, which act as natural barriers in the trench. The width of the trench sediments, the variable thickness of the infill along the trench (modified from Lohrmann et al. 2006), and the general transport direction of sediments in the trench are indicated (Völker et al. 2006). The sites of ODP leg 141 and ODP leg 202 site 1232 (Mix et al. 2003) are also indicated. **b** The geological map shows the principal distribution of late Palaeozoic (meta)sedimentary rocks and granites in the main Cordillera and the forearc. The main Cordillera acts as a continental divide and is mainly build up by the products of the late Mesozoic to Holocene arcs. The position of the Holocene volcanic arc is indicated by the volcanoes (map modified from SERNAGEOMIN 2003; Melnick and Echtler 2006). Sample locations of slope and trench sediments with respect to the position of the trench are also shown

marine forearc basins and the trench stem from the active arc and forearc (Fig. 1b). The oldest rocks west of the main Cordillera are of Devonian–Carboniferous to Triassic age and comprise the exposed accretionary complex of the Coastal Cordillera. Younger sequences of the accretionary complex are preserved in the offshore forearc, because the trench–arc geometry remained fairly stable throughout late Mesozoic and Cenozoic times (e.g. Duhart et al. 2001; Glodny et al. 2006 and references therein). Substantial erosion of the submarine forearc by subduction appears to be restricted to areas north of 36°S (e.g. Kay et al. 2005).

The accretionary complex is subdivided into an eastern and western series, which are separated by a NW–SE oriented fold (Fig. 1b). The W–E extension of the eastern series is ~100 km, that of the western series ~200 km. The latter comprises abundant siliciclastic (meta)sedimentary rocks from the high pressure–low temperature metamorphic regime of an accretionary wedge, which was accumulated between the latest Carboniferous to Triassic (Hervé 1988; Martin et al. 1999; Duhart et al. 2001; Willner et al. 2000; 2004; Glodny et al. 2005). The 200-km wide series includes some metabasites and (ultra)mafic rocks and forms the submarine part of the forearc. The eastern series comprises non-metamorphic to medium grade (meta)sedimentary rocks whereas high *P* metamorphism and metabasites are generally absent. The depositional age of these sediments is not well constrained, but they belong to Devonian–Carboniferous–Permian sedimentary basins along the western margin of Gondwana (González Bonorino 1991; França et al. 1995; López-Gamundi and Rossello 1998; Bandel and Quinzio-Sinn 1999). In contrast to the accretionary wedge of the Coastal Cordillera, Devonian metasedimentary rocks of the eastern foothills of the Main Cordillera are of the high-*T*, medium-*P* type (Lucassen et al. 2004).

Late Carboniferous to Permian granite batholiths intruded the Palaeozoic (meta)sedimentary sequence at shallow depth (e.g. Hervé et al. 1988; Martin et al. 1999; Lucassen et al. 2004) and scattered outcrops of granite are also found in the eastern part of the Main Cordillera (Fig. 1b, Caminos et al. 1988; Varela et al. 1994; Lucassen et al. 2004). The oldest Mesozoic magmatic rocks in the Coastal Cordillera are small late Triassic granites (Hervé et al. 1988; Lucassen et al. 2004). Subsequent abundant intrusive and volcanic rocks of the Jurassic to Holocene magmatic arc are mostly located in the Main Cordillera in Chile and Argentina (Fig. 1, e.g. López-Escobar 1984; Hickey et al. 1984; Hildreth and Moorbath 1988; Martin et al. 1999; south of 44°S see Pankhurst et al. 1999). Isolated Mesozoic and minor Mid-Tertiary magmatism also occurs west of the Main Cordillera (Martin et al. 1999; Muñoz et al. 2000). The intrusive rocks of the Main Cordillera form the northernmost part of the North Patagonian batholith, which extends to ca. 53°S (e.g. Pankhurst et al. 1999). The Plio-Pleistocene to Holocene arc volcanism in the Southern Volcanic Zone (SVZ) is mostly made up of basaltic andesite–andesite strato-volcanoes (e.g. López-Escobar 1984; Hickey et al. 1984; Hildreth and Moorbath 1988; Feeley et al. 1998). The Jurassic to present arcs remained at a near stationary position within the Main Cordillera and the trench-arc configuration shows no significant variation since approximately 200 Ma. This is in contrast to the evolutionary history of the Andean arcs north of 36°S.

The Palaeozoic (meta)sedimentary rocks and intrusions in the Coastal Cordillera are overlain by Triassic–Cretaceous sedimentary rocks (Ferraris 1981). The preservation of shallow-level late Palaeozoic intrusions and Triassic erosional unconformities indicate that denudation in the forearc was only in the range of a few km since the late Palaeozoic–early Mesozoic. Deeper sections of the crust are not exposed except in the accretionary complex of the Coastal Cordillera. Exhumation ceased in late Triassic times and low average rates of exhumation (0.03–0.04 mm/year) in the Coastal Cordillera between 200 Ma and Miocene were confirmed by fission track ages (Glodny et al. 2008).

A comprehensive study of the chemical and isotopic composition of the Palaeozoic to Tertiary metamorphic and magmatic basement between 41° and 36°S and a review of previous work was presented by Lucassen et al. (2004). The composition of the Pliocene to Holocene volcanic rocks from the Main Cordillera was studied by numerous authors (references see Fig. 2). Nd, Sr and Pb isotope compositions of (mid to late) Palaeozoic (meta)sedimentary and Palaeozoic granites are dominated by recycling of Proterozoic felsic continental crust. Nd–Sm model ages (Fig. 1b) vary between 1.3 and 2.1 Ga, in line with observations of similar rocks of comparable age between 50° and 21°S (e.g. Berg and Baumann 1985; Lucassen et al. 1999; Bock et al. 2000; Augustsson et al. 2006). In contrast to the recycled basement, isotope compositions of late Mesozoic to recent rocks of the arcs (in the following SVZ rocks; references see Fig. 2) indicate juvenile material from the relatively uniform sub-arc mantle and only small contributions of the ambient Palaeozoic basement.

Sampling, sample description and age of the ts-sediments

For this study we used bulk samples of unconsolidated sediment cores and dredge samples of hard rock outcrops. Cores were taken with a standard 1.5 to heavy gravity corer of 5–10 m length retrieving cores of 9 cm diameter. For hard rock outcrops we used a 1.0 × 0.4 m wide chain-bag dredge.

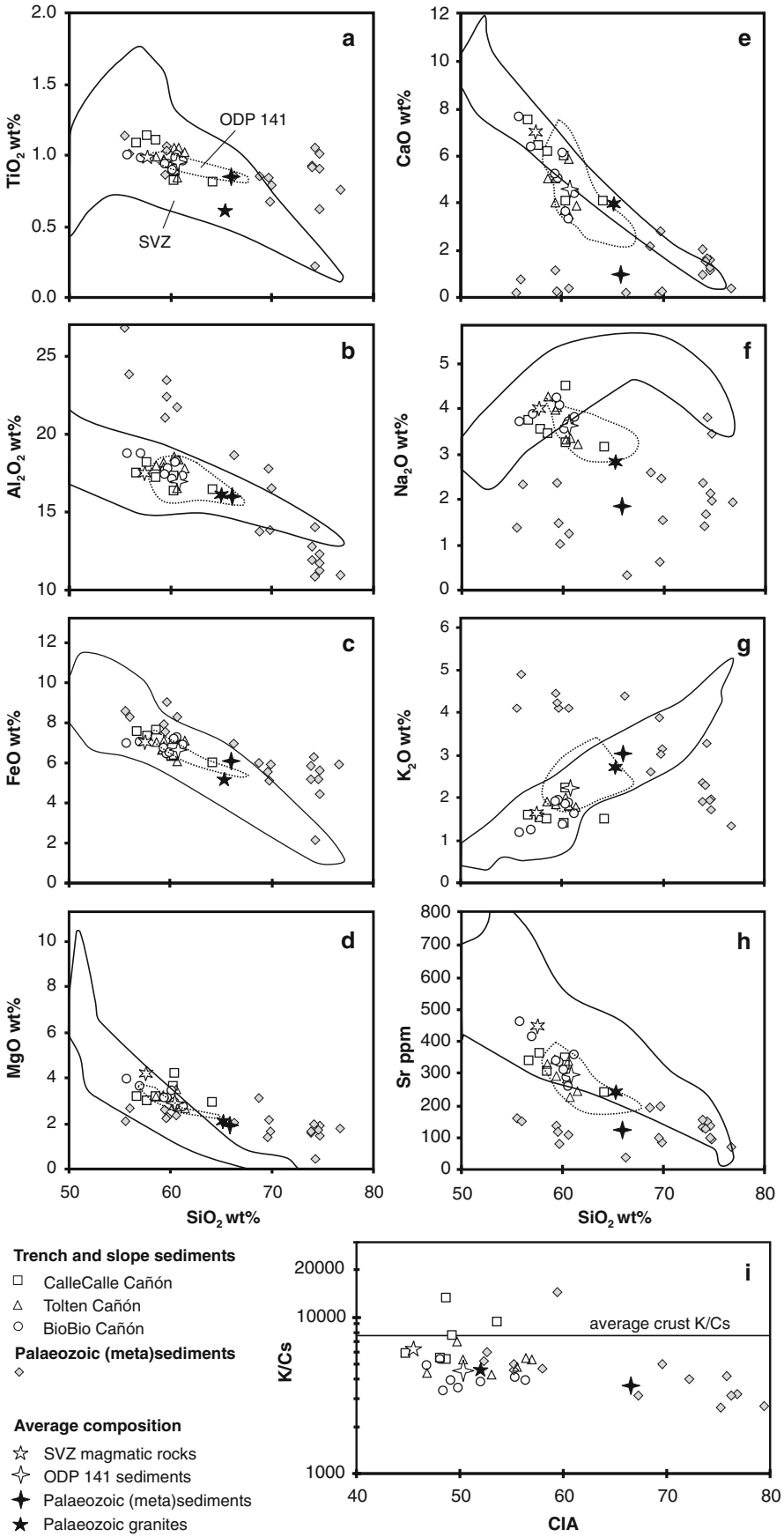

Fig. 2 Major element and Sr compositions and weathering index CIA (Chemical Index of Alteration; molar 100× [Al_2O_3/(Al_2O_3CaO+K_2O+Na_2O); fresh rocks <50; Nesbitt and Young 1982, 1984] of ts-sediments (ts = trench–slope) compared with the composition of the Palaeozoic basement [average composition of Palaeozoic granites and (meta)sediments and individual samples; Lucassen et al. 2004], sediments from the Chilean triple junction [ODP 141 sediments; compositional field (*dotted line*) and average; Kilian and Behrmann 2003], and SVZ rocks [compositional field (*solid line*) and average]. The Palaeozoic (meta)sedimentary rocks are an example of highly evolved sediments varying from clay to quartz dominated samples, whereas the ts-sediments including the ODP 141 samples from ~45°S represent immature sediments, which largely reflect the average composition of their sources. SVZ data: López-Escobar et al. 1981, 1992, 1995; Déruelle 1982; Frey et al. 1984; Hickey et al. 1986; Notsu et al. 1987; Hildreth and Moorbath 1988; Davidson et al. 1988; Gerlach et al. 1988; Grunder and Mahood 1988; Muñoz and Stern 1988; Hickey-Vargas et al. 1989; Ferguson et al. 1992; Tormey et al. 1995; López-Escobar and Vergara 1997; Muñoz et al. 2000; Lara et al. 2001; Dungan et al. 2001; Costa and Singer 2002; Lucassen et al. 2004; Jicha et al. 2007)

Samples were taken during RV SONNE cruise SO161-5 from 13 selected sites along the Chile trench and the neighboring lower to middle continental slope between latitudes 36° and 40°S (Fig. 1b; Table 1). Sampling locations concentrate near three submarine cañóns (CalleCalle: ~40–39°S; Tolten: ~39–38°S; BioBio: ~37–36°S) and provide material from two different geological units—(1) the present trench infill and (2) the lower slope sequence.

The present day trench fill was sampled using a gravity corer. Recovered cores are up to 8 m long. Sites were selected near the deformation front and in some distance to this structural lineament (Fig. 1b). To cover the slope sequence, several intraslope basins at the middle and lower slope were cored to define the composition of young and unconsolidated slope material. In addition, we dredged the steep escarpments of the deeply incised cañóns to recover consolidated and lithified (accreted?) sediments from somewhat older sequences, which form the lower slope.

From sediment cores commonly two separate bulk samples of 4–5 cm lengths and 60 g weight each were analyzed—one taken from an upper core meter and a second one near the core base. From dredged hard rock samples specimen of ~100–200 g weight were selected and processed for analyses.

Sedimentologically, samples comprise all variations of the clastic sequence—ranging from fine-grained silty mud to coarse graded sand beds and from mudstone to unsorted sandstones (details see Table 1). Commonly these lithologies stem from turbiditic sequences which are composed of an intercalation of mostly thin hemipelagic mud layers with silty to sandy, often graded turbidite beds. At slope locations we also sampled slumped clastic sequences which are mostly unsorted and also contain mud lenses. Occasionally lithified silt and sandstone slabs showed signs of tectonic strain. Additional information on sediments and their environmental interpretation can be found in the literature (Wiedicke et al. 2002; Völker et al. 2006, 2008; Raitzsch et al. 2007).

^{14}C-age determinations (sample 50SL from ~2.2 kyr at 0.2 m to 23 kyr at 7 m core depth; ODP leg 1232 from ~12 kyr at 0.6 m to 138 kyr at 96 m) and oxygen isotope stratigraphy of some of the cores (Blumberg et al. 2008; Völker et al. 2008) and dredge samples indicate variable Quaternary ages. Sediments from the gravity cores represent the late Pleistocene glaciation in the southern Andes; some samples have been assigned to the post-glacial Holocene (Table 1).

Chemical and isotopic composition of the ts-sediments and their possible sources

For the analytical procedures and data quality see the Appendix. Results of XRF and ICP-MS analyses and determinations of Sr, Nd, and Pb isotope ratios are presented in Table 2.

Chemical composition

The major element compositions of the ts-sediments are similar for samples of the three distant feeder systems (CalleCalle, Tolten, and BioBio Cañón; Fig. 1). TiO_2, Al_2O_3, FeO, MgO and K_2O contents are correlated with the SiO_2 contents (~56–64 wt%) following a gentle slope, whereas CaO and Na_2O (and Sr) vary independently from SiO_2.

In order to compare the major element composition of the ts-sediments with possible sources, we include published data of Palaeozoic granites and (meta)sedimentary rocks, and SVZ rocks (Fig. 2). The composition of the ts-sediments—except for the more variable CaO, Na_2O and Sr contents—mainly plot into the field of the SVZ rocks close to the average of the latter. The variation of CaO, Na_2O, and Sr contents is most likely caused by weathering of plagioclase (e.g. Nesbitt and Young 1984; McLennan et al. 1990), which also dominates the weathering index (Fig. 2i). The composition of the Palaeozoic basement especially of the Palaeozoic (meta)sedimentary rocks, is different. Significant contributions from these rocks to the major element compositions of the ts-sediments are unlikely (Fig. 2). In contrast, the composition of the ts-sediments and ODP Leg 141 sediments is fairly similar (Fig. 2). Both are—compared with the Palaeozoic (meta)sedimentary rocks—immature (Fig. 2i) and reflect largely the major element compositions of their sources.

Variation of trace element contents in the ts-sediments is moderate, which is indicated by the small compositional field (Fig. 3a). The average pattern of the ts-sediments resembles the pattern of a variety of rocks including the ODP Leg 141 sediments, SVZ rocks, average Global Subducted Sediment (GLOSS; Plank and Langmuir 1998) as a proxy for upper crust composition and even the most distinct pattern of the Palaeozoic (meta)sedimentary rocks is similar (Fig. 3a). The main difference between the REE patterns of the average ts-sediment ($La/Yb_{normalized}$ ~5) and SVZ rocks ($La/Yb_{normalized}$ ~4.5) is the slightly higher REE content of the latter (Fig. 3b). The average REE patterns ($La/Yb_{normalized}$ ~9) of the Palaeozoic granite and Palaeozoic (meta)sedimentary rocks are broadly similar and the main difference between the ts-sediments and Palaeozoic basement is the slightly higher REE concentration of the latter (Fig. 3b).

Sr, Nd, and Pb isotope signatures

Isotope compositional ranges (Fig. 4a–c) of the ts-sediments are relatively small with $^{87}Sr/^{86}Sr$ ~0.7041–0.7061,

Table 1 Locations and settings of sampling sites and their lithological characteristics

Sample identifier	Latitude/longitude	Water depth (m); setting	Rock type	Estimated age (base of core)
(40°S) South to North (36°S)				
31 SL (1) 784–789 cm 31 SL (2) 684–689 cm	36°04.1′S/74°04.6′W	4,959 m; trench infill near deformation front	Thin silty to fine sandy turbidites intercalated with thin hemipelagic mud layers; with pellets, some forams	Late Pleistocene
115 KD	36°40′S/74°12.3′W	3,450 m; south flank of BioBio canyon at lower slope, near canyon mouth	Tan-gray massive friable mudstone	Quaternary
32 KD	36°39.4′S/74°11′W	3,500 m; flank of BioBio canyon; lower slope close to deformation front	Clay-rich fine-grained massive litharenite (volcanoclastic sandstone)	Quaternary
33 SL (1) 5–10 cm 33 SL (2) 54–58 cm	36°44.5′S/74°25′W	4,550 m; levee within trench; near mouth of BioBio canyon	Medium coarse-grained sandy turbidite (4-cm thick sand layers) Intercalated silty hemipelagic and fine-medium grained sand turbiditc layers	Holocene (?)
113 SL (1) 270–275 cm 113 SL (2) 460–465 cm	36°58.4′S/74°10′W	3,182 m; intraslope basin	Turbiditic infill in intraslope basin (intercalation of thin sandy turbidites with silty–muddy hemipelagic layers	Early Holocene
112 SL (1) 328–333 cm 112 SL (2) 504–509 cm	38°04.8′ S/74°29.8′ W	4,130 m; confined basin at foot of continental slope (particularly large catchment area of the slope)	Dominantly silty clay to pelletal silt, intercalated with sand layers (a rapidly deposited turbiditic sequence)	<1 ky (late Holocene)
50 SL (1) 635–640 cm 50 SL (2) 704–709 cm	38°18.8′S/74°41.9′W	4,380 m, small topographic high within trench; close to foot of slope	Intercalation of hemipelagic mud and thin graded silt to sand layers (distal and fine-grained turbiditic sequence of the trench fill)	Ca. 30 ky (late Pleistocene)
100 SL (1) 315–320 cm 100 SL (2) 375–380 cm	38°30.6′ S/74°57.9′ W	4,223 m; small topographic high within trench, distant to foot of slope	Intercalation of clayey mud and thin silt to sand layers (distal fine-grained turbiditic trench sequence)	Late Pleistocene
57 KD	38°44′S/74°37.1′W	Lower continental slope near deformation front, near Tolten canyon	Sandy, dark mudstone grading into muddy sandstone	Quaternary
70 KD	39°37′ S/74°46.1′ W	2,998 m; flank of topographic high in slope setting	Consolidated silty mud, with angular clasts, faecal pellets, and few thin black turbiditic sand layers	Quaternary
75 KD, 1 75 KD, 2	39°54.5′S/74°48.6′W	3,250 m; escarpment at lower slope	Volcanoclastic sandstone (coarse-grained litharenite), no stratification Fine-grained dark-gray silty sandstone	Quaternary
90 SL (1) 177–180 cm 90 SL (2) 311–315 cm	39°51.4′S/74°47.7′W	2,659 m; local high at middle part of slope	Hemipelagic sandy mud including fine sandy turbidite layers Intercalation of sandy turbidites with hemipelagic mud	Quaternary
97 KD	39°53.8′S/74°51.4′W	3,700 m; frontal escarpment of lower continental slope (near deformation front), south of CalleCalle canyon near Bueno canyon	Poorly sorted sandstone (polymictic lithic wacke), tectonized (with fractures)	Quaternary

Table 2 Whole rock major (wt%) and trace (ppm) element and isotope composition

Sample	70 KD	75 KD (1)	75 KD (2)	97 KD	90 SL (1)	90 SL (2)	100 SL (2)
SiO_2	54.3	62.0	58.0	56.5	51.8	55.2	55.4
TiO_2	1.1	0.8	0.8	0.8	1.0	1.0	1.0
Al_2O_3	17.1	15.9	16.6	15.3	16.0	16.2	17.0
Fe_2O_3	7.6	6.4	6.8	6.7	7.7	8.0	7.4
MnO	0.1	0.1	0.1	0.1	0.1	0.1	0.1
MgO	2.8	2.8	3.5	3.9	2.9	3.0	2.6
CaO	6.0	4.0	5.8	3.8	6.9	5.8	3.4
Na_2O	3.3	3.0	3.1	4.2	3.4	3.2	3.1
K_2O	1.4	1.4	1.4	2.1	1.4	1.4	1.8
P_2O_5	0.2	0.1	0.1	0.2	0.2	0.2	0.2
LOI	5.9	4.7	4.6	6.4	6.6	5.6	6.1
Total	99.9	101.3	100.8	100.0	98.1	99.9	98.0
Ba	390	294	296	307	542	452	466
Rb	36	34	30	36	35	34	52
Sr	397	272	382	359	371	337	270
Cr	56	44	69	81	61	61	66
Ni	31	19	24	32	31	28	23
Ga	20	16	16	14	16	16	19
V	181	130	162	161	176	188	173
Zn	94	71	62	65	90	88	88
Zr	130	147	127	128	132	132	145
Y[a]	21.8	16.3	14.8	16.7	20.0	21.5	18.2
Nb[a]	4.52	5.00	3.25	4.26	4.87	4.75	5.29
Cs[a]	2.38	1.33	1.53	1.40	2.24	2.27	3.11
La[a]	14.4	13.5	12.3	12.3	14.1	14.2	14.6
Ce[a]	32.5	29.7	26.6	26.8	32.5	31.8	33.1
Pr[a]	4.27	3.71	3.39	3.41	4.03	4.08	4.10
Nd[a]	18.1	15.6	14.0	13.9	17.1	17.3	17.0
Sm[a]	4.18	3.54	3.05	3.27	3.89	4.06	3.82
Eu[a]	1.16	0.98	0.88	0.93	1.05	1.12	1.02
Gd	4.16	3.41	2.91	3.21	3.90	3.99	3.63
Tb[a]	0.66	0.54	0.45	0.49	0.61	0.66	0.58
Dy[a]	4.10	3.31	2.79	3.10	3.81	4.00	3.49
Ho[a]	0.84	0.67	0.58	0.64	0.79	0.82	0.73
Er[a]	2.44	1.93	1.67	1.85	2.29	2.39	2.18
Tm[a]	0.36	0.28	0.24	0.26	0.32	0.36	0.31
Yb[a]	2.32	1.91	1.57	1.72	2.18	2.33	2.07
Lu[a]	0.35	0.29	0.25	0.26	0.33	0.35	0.32
Hf[a]	2.74	2.75	2.02	2.06	2.66	2.69	2.99
Ta[a]	0.33	0.37	0.25	0.32	0.40	0.33	0.39
Pb[a]	11.3	7.99	8.88	7.02	11.2	11.3	13.2
Th[a]	3.84	4.22	4.16	3.55	4.09	3.95	4.97
U[a]	3.34	1.06	1.81	0.82	2.10	1.62	3.25
$^{87}Sr/^{86}Sr$	0.705014 ± 7	0.705637 ± 8	0.704605 ± 8	0.705409 ± 8	0.706186 ± 10	0.705483 ± 6	0.705777 ± 6
$^{87}Sr/^{86}Sr$[b]	0.709111 ± 9				0.709157 ± 9	0.709117 ± 9	
$^{143}Nd/^{144}Nd$	0.512729 ± 6	0.512673 ± 8	0.512780 ± 6	0.512709 ± 4	0.512714 ± 6	0.512744 ± 5	0.512709 ± 4
$^{206}Pb/^{204}Pb$	18.62	18.71	18.60	18.67	18.63	18.63	18.62
$^{207}Pb/^{204}Pb$	15.62	15.63	15.61	15.62	15.62	15.62	15.62
$^{208}Pb/^{204}Pb$	38.56	38.65	38.52	38.61	38.56	38.56	38.58

Table 2 continued

Sample	112 SL (1)	112 SL (2)	50 SL (1)	50 SL(2)	57 KD	100 SL (1)	113 SL (1)
SiO_2	54.2	55.3	55.8	55.0	57.9	54.4	52.4
TiO_2	0.9	0.9	0.9	0.9	0.8	0.9	0.9
Al_2O_3	16.4	16.0	16.8	16.9	15.9	16.7	15.8
Fe_2O_3	7.2	7.1	7.0	7.4	6.5	7.3	7.0
MnO	0.1	0.1	0.1	0.1	0.1	0.1	0.1
MgO	2.5	2.4	3.0	3.0	3.3	3.0	2.4
CaO	3.1	3.5	4.7	3.7	5.6	4.7	2.8
Na_2O	3.0	2.9	3.7	3.8	3.6	4.0	3.2
K_2O	1.6	1.6	1.7	1.8	1.7	1.8	1.6
P_2O_5	0.2	0.2	0.2	0.2	0.1	0.2	0.2
LOI	7.6	7.3	4.1	5.5	2.8	5.6	12.1
Total	96.9	97.2	98.1	98.2	98.3	98.5	98.5
Ba	497	403	454	437	376	468	612
Rb	48	46	50	59	54	47	51
Sr	256	273	335	282	333	315	258
Cr	83	79	66	57	57	65	77
Ni	29	26					35
Ga	18	18	20	20	14	17	18
V	157	145	163	161	169	150	132
Zn	94	87	78	74	54	80	111
Zr	136	144	124	124	122	125	130
Y[a]	17.3	17.8	21.8	21.5	19.4	22.3	16.3
Nb[a]	5.22	5.19	8.8	8.4	7	7.7	4.89
Cs[a]	3.18	2.75	3.58	3.7	2.17	3.59	4.02
La[a]	13.8	13.9	17.7	16.7	13.5	16.5	13.2
Ce[a]	30.8	31.3	38.5	37.3	29.6	36.8	29.0
Pr[a]	3.89	3.96	4.8	4.6	3.76	4.7	3.68
Nd[a]	16.1	16.6	20	19.3	16	19.6	15.1
Sm[a]	3.64	3.73	4.52	4.39	3.8	4.44	3.38
Eu[a]	0.97	1.00	1.2	1.14	1.05	1.21	0.89
Gd	3.42	3.51	4.39	4.27	3.77	4.27	3.07
Tb[a]	0.52	0.54	0.68	0.65	0.59	0.66	0.49
Dy[a]	3.29	3.38	4.13	4.04	3.65	4.18	3.06
Ho[a]	0.68	0.69	0.81	0.79	0.72	0.83	0.62
Er[a]	2.01	2.02	2.54	2.38	2.23	2.5	1.80
Tm[a]	0.29	0.29	0.34	0.32	0.3	0.37	0.26
Yb[a]	1.96	1.93	2.28	2.29	2.05	2.38	1.80
Lu[a]	0.30	0.30	0.34	0.33	0.32	0.36	0.28
Hf[a]	2.75	2.57	3.72	3.65	1.94	3.82	2.78
Ta[a]	0.37	0.36	4.5	2.5	2.1	2.1	0.35
Pb[a]	11.8	11.2	15.8	25	8.9	16.1	12.3
Th[a]	4.80	4.54	5.52	5.5	3.49	5.23	4.88
U[a]	2.08	1.96	1.8	2.41	1.05	3.48	2.64
$^{87}Sr/^{86}Sr$	0.705632 ± 6	0.705413 ± 11	0.704860 ± 10	0.705360 ± 10	0.705369 ± 10	0.705261 ± 10	0.705475 ± 8
$^{87}Sr/^{86}Sr$[b]		0.709038 ± 9	0.709114 ± 10				
$^{143}Nd/^{144}Nd$	0.512704 ± 5	0.512699 ± 6	0.512787 ± 5	0.512733 ± 5	0.512723 ± 6	0.512734 ± 5	0.512710 ± 6
$^{206}Pb/^{204}Pb$	18.63	18.63	18.60	18.62	18.63	18.62	18.62
$^{207}Pb/^{204}Pb$	15.63	15.62	15.62	15.62	15.62	15.63	15.61
$^{208}Pb/^{204}Pb$	38.61	38.56	38.55	38.56	38.57	38.58	38.53

Table 2 continued

Sample	113 SL (2)	31 SL (1)	31 SL (2)	32 KD	33 SL (1)	33 SL (2)	115 kd
SiO_2	52.9	54.9	54.0	58.1	52.9	54.7	57.4
TiO_2	0.9	0.9	0.9	0.9	1.0	0.9	0.9
Al_2O_3	16.0	16.4	15.8	16.5	17.8	18.0	16.2
Fe_2O_3	7.0	6.6	6.8	6.9	7.3	7.5	7.2
MnO	0.1	0.1	0.1	0.1	0.1	0.1	0.1
MgO	2.6	2.8	2.8	3.3	3.7	3.5	2.5
CaO	3.2	4.6	4.8	5.9	7.3	6.1	4.1
Na_2O	3.2	3.7	3.8	3.4	3.5	3.7	3.6
K_2O	1.6	1.8	1.7	1.3	1.1	1.2	1.5
P_2O_5	0.2	0.2	0.2	0.1	0.2	0.2	0.2
LOI	11.5	6.2	7.4	1.8	1.4	5.0	4.7
Total	99.1	98.2	98.2	98.4	96.2	100.9	98.5
Ba	653	512	550	327	307	396	343
Rb	48	52	56	43	30	33	42
Sr	287	335	340	312	462	416	358
Cr	74	65	60	86	82	94	63
Ni	31			21	23	27	
Ga	16	19	16	18	19	14	16
V	135	146	151	174	173	169	130
Zn	106	83	83	63	66	74	79
Zr	131	122	123	118	102	105	120
Y[a]	16.4	20.6	20.3	20.8	18.2	19.1	21.2
Nb[a]	4.58	8.3	8.1	7.4	6.3	6.2	6.8
Cs[a]	3.79	4.56	4.74	2.09	1.98	2.65	3.51
La[a]	12.9	16.6	16.5	14.2	12.5	13.7	14.9
Ce[a]	28.7	36.5	36.7	31.1	27.7	30.6	33.2
Pr[a]	3.68	4.57	4.58	3.84	3.64	3.97	4.31
Nd[a]	15.3	19	18.7	16.8	15.9	16.9	18.5
Sm[a]	3.41	4.2	4.23	3.84	3.69	3.9	4.21
Eu[a]	0.92	1.12	1.1	1.06	1.13	1.12	1.16
Gd	3.24	3.99	4.1	3.98	3.73	3.86	4.13
Tb[a]	0.48	0.62	0.59	0.63	0.56	0.58	0.67
Dy[a]	3.12	3.75	3.74	3.81	3.29	3.53	3.83
Ho[a]	0.64	0.78	0.74	0.81	0.66	0.71	0.79
Er[a]	1.87	2.23	2.25	2.34	1.97	2.09	2.36
Tm[a]	0.28	0.32	0.32	0.33	0.27	0.3	0.33
Yb[a]	1.83	2.13	2.14	2.21	1.92	2.04	2.22
Lu[a]	0.28	0.31	0.33	0.34	0.28	0.29	0.35
Hf[a]	2.71	3.72	3.8	2.4	2.92	3.51	3.68
Ta[a]	0.32	3.5	2.2	2.5	3.1	1.9	1.6
Pb[a]	11.7	26	25.6	9.49	8.56	11.5	12.8
Th[a]	4.55	5.61	5.75	4.39	3.22	3.74	4.47
U[a]	2.85	2.22	2.27	2.86	1.05	1.86	1.36
$^{87}Sr/^{86}Sr$	0.705173 ± 8	0.705057 ± 10	0.705411 ± 8	0.704940 ± 10	0.704153 ± 14	0.704407 ± 10	0.704833 ± 7
$^{87}Sr/^{86}Sr$[b]		0.708929 ± 7			0.709088 ± 7		
$^{143}Nd/^{144}Nd$	0.512707 ± 5	0.512763 ± 5	0.512748 ± 8	0.512748 ± 5	0.512787 ± 5	0.512767 ± 5	0.512775 ± 6
$^{206}Pb/^{204}Pb$	18.63	18.61		18.64	18.57	18.60	18.60

?Table 2 continued

Sample	70 KD	75 KD (1)	75 KD (2)	97 KD	90 SL (1)	90 SL (2)	100 SL (2)
$^{207}Pb/^{204}Pb$	15.63	15.62		15.62	15.62	15.63	15.62
$^{208}Pb/^{204}Pb$	38.60	38.59		38.57	38.52	38.56	38.54

Errors on Sr and Nd isotope ratios are quoted as 2σ (m), assumed error on Pb isotope ratios <0.1%

[a] Measured by ICP-MS

[b] $^{87}Sr/^{86}Sr$ on pore-water

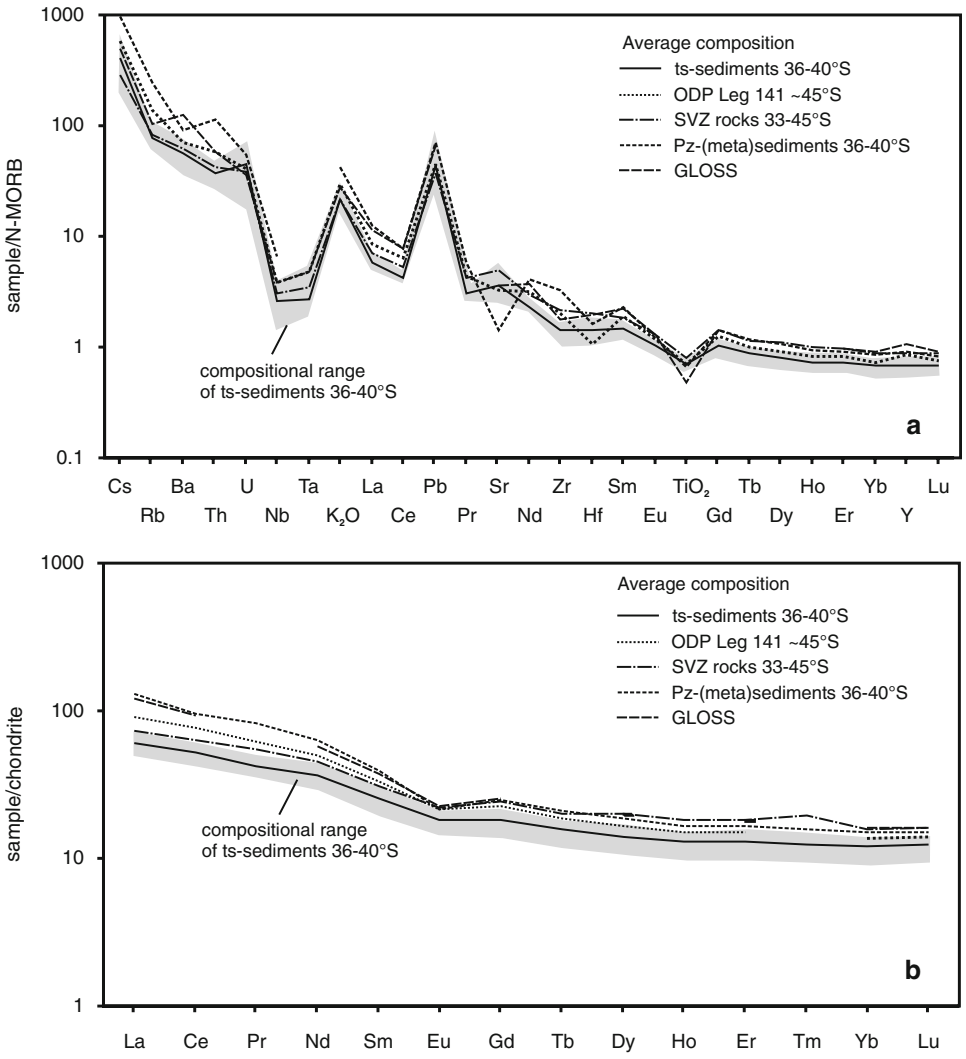

Fig. 3 **a** Average trace element distribution patterns including K_2O and TiO_2 of the different types of sediments in the area and rocks from the Southern Volcanic Zone (SVZ); normalized to N-MORB (Sun and McDonough 1989). The *shaded area* represents the compositional range of the 21 ts-sediment samples. **b** Average REE element patterns and compositional range of the ts-sediments; normalized to C1 chondrite (McDonough and Sun 1995). Data sources see Fig. 2; GLOSS (global subducted sediment) from Plank and Langmuir (1998)

$^{143}Nd/^{144}Nd$ ~0.51267–0.51278, $^{206}Pb/^{204}Pb$ ~18.57–18.71, $^{207}Pb/^{204}Pb$ ~15.61–15.63, and $^{208}Pb/^{204}Pb$ ~38.51–38.61. There are neither systematic differences between the three sample areas nor are they related to the water depth, i.e. slope or trench position of the sample locality, or to the presumed ages. Sr isotopes measured on the washing water of seven samples are different from the whole rock values and vary between ~0.7089 and 0.7092, i.e. the composition of the pore water is close to present Sr isotope composition of seawater (0.70907; Burke et al. 1982).

Isotope composition of the ts-sediments is distinct from those of the average Palaeozoic granite and (meta)sedimentary rocks, GLOSS, and ODP 141 sediments (Fig. 4). The differences between average SVZ rocks and ts-sediment compositions are small for all isotope systems (Fig. 4). The small compositional deviations of the ts-sediments appear to be systematic and can be described by binary mixing. Using the average isotope compositions and Sr, Nd, and Pb contents of average SVZ rocks and Palaeozoic (meta)sedimentary rocks as mixing endmembers, the Sr, Nd and Pb isotope

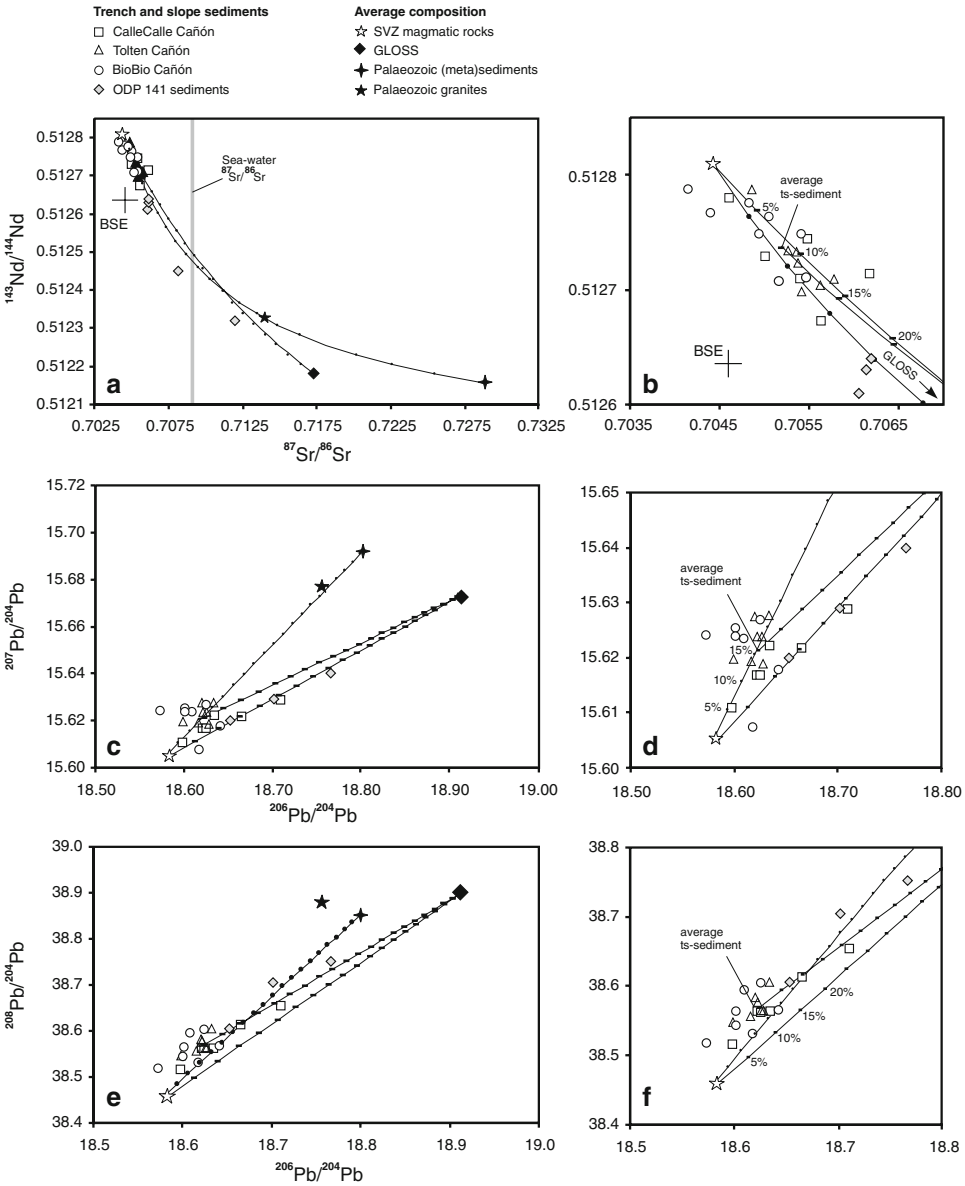

Fig. 4 Sr, Nd, and Pb isotope composition of ts-sediments, ODP 141 sediments and average compositions of possible sources. *Tick marks* on the binary mixing lines between SVZ magmatic rocks and Palaeozoic-(meta)sediments indicate 5% steps; *other lines* show the mixing trajectory between SVZ magmatic rocks and average ts-sediments and GLOSS for comparison. **a**, **b** Sr and Nd isotope composition; **c**, **d** $^{207}Pb/^{204}Pb$–$^{206}Pb/^{204}Pb$; **e**, **f** $^{208}Pb/^{204}Pb$–$^{206}Pb/^{204}Pb$. Data sources see Figs. 2 and 3

compositions of the ts-sediments are explained by variable addition of ~0–20% of the respective elements from Palaeozoic (meta)sedimentary rocks to the average SVZ-rock (Fig. 4). The average composition of Palaeozoic granites plots on or close to the mixing lines and indicates a prominent contribution of Palaeozoic (meta)sedimentary crust in these rocks (Fig. 4; Lucassen et al. 2004). Therefore, contributions from the Palaeozoic granites would be difficult to trace in the isotope signature of the ts-sediments.

Discussion

Chemical and isotopic composition

The major element composition of the ts-sediments reflects mainly the averaged compositions of SVZ rocks, which is andesite in transition to basaltic andesite (Fig. 2). Systematic deviations of ts-sediment's element composition from the compositional trends of the arc magmatic rocks restrict to the loss of Ca, Na, and Sr, which indicates weathering or transport-selection of plagioclase. The overall effect the latter is low to moderate (Fig. 2i) and the compositional range is small compared with the highly evolved rocks, e.g. the Palaeozoic (meta)sedimentary rocks (Fig. 2). Erosion of the material and transport was likely a fast process along the steep gradient from the mountain range to the trench. The high TiO_2 (~1.5–2.0 wt%) and P_2O_5 (~0.3–0.8 wt%) contents, which were reported for vitric clasts in various ts-sediment samples of similar SiO_2 and $Na_2O + K_2O$ composition (Völker et al. 2006 including samples KD 32, SL 33, and SL 50 of this study) are not reproduced by the whole rock analyses. The vitric

clasts are not dominant in the ts-sediments investigated here. Trace element patterns of the ts-sediments and their potential sources show minor differences and there is little chance to quantify the contributions of the various sources to individual samples by their trace element signatures (Fig. 3).

The isotope composition of ts-sediments is dominated by the composition of the SVZ rocks and the contribution of Palaeozoic basement is less than 20% (Fig. 4). Alteration by seawater cannot be discerned in the Sr isotope composition of the washed ts-sediments (Fig. 4a). Systematic incorporation of Sr derived from the seawater into silicate minerals obviously does not occur at least in the uppermost section of the sedimentary pile, which is represented by the piston cores. Influence of seawater Sr isotope signatures is also not evident in the solidified samples. Oceanic sediments from pelagic sedimentation on the oceanic plate should be different in isotopic composition and have been shown to reflect upper crust compositions in average (GLOSS; Plank and Langmuir 1998). In absence of data on the geochemical composition of the incoming oceanic sediments, we assume a composition similar to GLOSS for the sedimentary cover of the Nazca plate (Fig. 1a). The addition of oceanic sediments to the subduction system has been inferred from the interpretation of multichannel seismic data in the sediment pile (Reichert and Schreckenberger 2002; Völker et al. 2006). The near-surface sediments, however, appear to be dominated by turbidite deposits from the slope, which cover the trench–plane and parts of the seaward trench–slope (Völker et al. 2006). Small contributions of GLOSS would be difficult to distinguish from small contributions of Palaeozoic basement in the Sr–Nd isotope system of our samples (Fig. 4a). The Pb isotope compositions of the ODP 141 sediments (and their Sr–Nd isotope) and of two of our samples indicate the possible influence of a source different from the Palaeozoic basement, but the mixing patterns of uranogenic Pb (Fig. 4c, d) and thorogenic Pb (Fig. 4e, f) do not consistently indicate a GLOSS component. Possible contributions from an oceanic sedimentary source remain speculative.

The small compositional variations of the ts-sediments are not related to the variable W–E outcrop widths of the Palaeozoic series, which is 200 km south of 38°S and 100 km towards the North. Possible sediment transport from South to North along the Chile trench (Fig. 1a; Völker et al. 2006) is not evident in the composition of the samples.

Long-term evolution

Recent work on the exhumation history of the arc and forearc area of the studied section and its southern continuation reveals a strong geographic segmentation based on zircon and apatite fission track ages. The Palaeozoic basement of the forearc was already exhumed to depths <2 km in late Cretaceous, according to apatite fission track ages, which record the latest stage of the thermal history. Averaged exhumation rates were low in the western and eastern series (0.04 mm/a; Glodny et al. 2008). The only exception to this scheme is the young Pliocene to Holocene uplift of a Palaeozoic granite massif in the Coastal Cordillera ~37–38°S (Fig. 1b; Nahuelbuta Range; Melnick and Echtler 2006; Glodny et al. 2008) and the rare occurrences of Palaeozoic basement rocks within the Main Cordillera (Fig. 1b). Apatite fission track ages in the magmatic arc of the Main Cordillera indicate rapid exhumation from Pliocene to Recent south of 39°S (up to 2 mm/a), whereas the exhumation rates decreased towards the North and are up to one order of magnitude lower at 36°S (Thomson 2002; Glodny et al. 2008). The gradient is mainly related to latitudinally variable glaciation/deglaciation effects, which occur episodically since ca 6 My in the Main Cordillera and variable precipitation, which are both more intense towards the South and promote the high sedimentation rates in the trench (e.g. Lamy et al. 2001; Kilian and Behrmann 2003; Melnick and Echtler 2006; Thomson 2002; Glodny et al. 2006). The chemical and isotope composition of the ts-sediments is not affected by this exhumation pattern and the mixing ratios of Palaeozoic basement and SVZ rocks are indistinguishable at 40° and 36°S. Site 1232 of ODP leg 202 comprises ~362 m of lithological uniform turbidite deposits shed from the continental slope with a basal age of 780 kyr (Mix et al. 2003). The lithology of the gravity cores used in this study and the extended profile of site 1232 are similar and indicate similar deposition–source relationships on an extended time scale.

The dominance of detritus from the SVZ rocks in the continental sedimentary input is likely a stable feature at a time scale longer than that calculated for the subduction of sediment from the trench down to the depth of fluid–melt generation and eclogite formation. Subduction velocity similar to the averaged rates (80 mm/year; Somoza 1998) and the present convergence rates (66 mm/year; Angermann et al. 1999) respectively transport continental sediments from the trench to depth of ~100 km in ~3.4–4 My. Subducted sediments presently in the zone of fluid–melt and eclogite generation are of early Pliocene to late Miocene age. The low average long-term exhumation of the Palaeozoic western and eastern series combined with the evidence for pre-Pliocene exhumation of the Main Cordillera (Glodny et al. 2006, 2008 and references therein) after the late Oligocene/early Miocene reorganization of the oceanic plate (e.g. Tebbens and Cande 1997) opens a long-term perspective for the continental sedimentary contribution to the

subduction system from early Miocene onwards. SVZ magmatic rocks older than the late Miocene to Holocene volcanic rocks comprise abundant late Cretaceous to Miocene intrusions. Holocene to Cretaceous magmatic rocks show all similar primitive arc signature (e.g. Lucassen et al. 2004). Most likely, since ~20 Ma arc material was the prevailing component of continental contributions to slope and trench sediments.

Acknowledgments We thank Maren Lewerenz for performing XRF analyses at the Technische Universität Berlin, Peter Dulski and Birgit Zander for ICP-MS analyses at GFZ-Potsdam, Cathrin Schulz for support in the GFZ radiogenic isotope laboratory, Rosemarie Geffe at TU-Berlin for polishing the Figures. We thank Rolf L. Romer for reading a previous draft of the manuscript and Christoph Breitkreuz and Diego Morata for their journal reviews, which all improved the manuscript. This study was funded by DFG (Deutsche Forschungsgemeinschaft) in the frame of Sonderforschungsbereich 267 'Deformation processes in the Andes'.

Appendix

Analytical methods

The initial sample size was ca. 50 g, which is representative even for the sand fraction. Semi-solidified rocks from the dredge samples were carefully disaggregated in a PE-bag using a hammer. All samples where transferred into Teflon beakers, washed several times in the ultrasonic in ultra clean water and dried. The water was preserved (with few drops HCl added). The dried samples were ground in an agate mill. Major elements were determined by XRF at TU-Berlin. Trace elements were determined by ICP-MS at GFZ-Potsdam (for the procedure and reproducibility of international standards see Dulski 2001).

For Nd, Pb, and Sr isotope analyses by TIMS at GFZ Potsdam, ~200 mg of sample were weighted into Savillex beakers. Prior to dissolution in HF–HNO_3 mixture, the samples were treated with warm 1 N HCl followed by washing in ultra clean water in order to remove possible organic carbonates. All isotope ratios were determined using TIMS. Nd and Sr isotope ratios were measured using dynamic multi-collection on a MAT 262 mass spectrometer and on a VG 54 Sector mass spectrometer at the GFZ-Potsdam, respectively. Nd isotopic ratios were normalized to $^{146}Nd/^{144}Nd = 0.7219$, Sr isotopic ratios to $^{86}Sr/^{88}Sr = 0.1194$. During the analytical work at GFZ-Potsdam the NBS 987 Sr standard yielded $^{87}Sr/^{86}Sr = 0.710265 \pm 28$ (2σ; $n = 47$) and the La Jolla Nd standard yielded $^{143}Nd/^{144}Nd = 0.511850 \pm 8$ (2σ, $n = 46$). Pb isotope ratios were measured at GFZ-Potsdam using static multi-collection on a MAT 262 mass spectrometer at controlled temperatures between 1,220 and 1,250°C. The 2σ reproducibility of all Pb isotope ratios of the NBS SRM 981 standard (measured ratios, uncorrected for fractionation; $^{206}Pb/^{204}Pb = 16.906 \pm 10$, $^{207}Pb/^{204}Pb = 14.454 \pm 10$, $^{208}Pb/^{204}Pb = 36.583 \pm 20$, $n = 28$) is better than 0.1% and a 2σ error of 0.1% is assumed for the measured samples considering the uncertainty of correction for mass fractionation. Instrumental mass-fractionation has been corrected using 0.1% per amu (atomic mass unit) on the base of the NBS SRM 981 values. Procedural blanks were <30 pg for Pb, <50 pg Nd and <100 pg for Sr. No blank corrections have been applied to the measured ratios because blank contribution was insignificant in comparison to the amount of the respective elements in the sample.

References

Angermann D, Klotz J, Reigber C (1999) Space-geodetic estimation of the Nazca-South America Euler vector. Earth Planet Sci Lett 171:329–334. doi:10.1016/S0012-821X(99)00173-9

Augustsson C, Münker C, Bahlburg H, Fanning M (2006) Provenance of late Palaeozoic metasediments of the SW South American Gondwana margin: a combined U–Pb and Hf-isotope study of single detrital zircons. J Geol Soc Lond 163:983–995. doi:10.1144/0016-76492005-149

Bandel K, Quinzio-Sinn LA (1999) Paleozoic trace fossils from the Cordillera Costal near Concepción, connected to a review of the Paleozoic history of central Chile. Neues Jahrb Geol Palaeontol Abh 211:171–200

Behrmann JH, Kopf A (2001) Balance of tectonically accreted and subducted sediment at the Chile Triple Junction. Int J Earth Sci 90:753–768. doi:10.1007/s005310000172

Berg K, Baumann A (1985) Plutonic and metasedimentary rocks from the Coastal range of northern Chile: Rb–Sr and U–Pb isotopic systematics. Earth Planet Sci Lett 75:101–115. doi:10.1016/0012-821X(85)90093-7

Blumberg S, Lamy F, Arz HW, Echtler HP, Wiedicke M, Haug GH, Oncken O (2008) Turbiditic trench deposits at the South-Chilean active margin: a Pleistocene–Holocene record of climate and tectonics. Earth Planet Sci Lett. doi:10.1016/j.epsl.2008.02.007

Bock B, Bahlburg H, Wörner G, Zimmermann U (2000) Tracing crustal evolution in the southern Central Andes from Late Precambrian to Permian using Nd and Pb isotopes. J Geol 108:515–535. doi:10.1086/314422

Burke WH, Denison RE, Hetherington EA, Koepnick RB, Nelson HF, Otto JB (1982) Variation of seawater $^{87}Sr/^{86}Sr$ throughout Phanerozoic time. Geology 10:516–519. doi:10.1130/0091-7613(1982)10<516:VOSSTP>2.0.CO;2

Caminos R, Llambías EJ, Rapela CW, Párica CA (1988) Late Paleozoic-Early Triassic magmatic activity of Argentina and the significance of new Rb–Sr ages from northern Patagonia. J S Am Earth Sci 1:137–145. doi:10.1016/0895-9811(88)90031-4

Costa F, Singer BS (2002) Evolution of Holocene dacite and compositionally zoned magma, volcan San Pedro, southern volcanic zone Chile. J Petrol 43:1571–1593. doi:10.1093/petrology/43.8.1571

Davidson JP, Ferguson KM, Colucci MT, Dungan MA (1988) The origin and evolution of magmas from the San Pedro-Pellado volcanic complex, S Chile: multicomponent sources and open system evolution. Contrib Miner Petrol 100:429–445. doi:10.1007/BF00371373

Déruelle B (1982) Petrology of the Plio-Quaternary volcanism of the south-central and meridional Andes. J Volcanol Geotherm Res 14:77–124. doi:10.1016/0377-0273(82)90044-0

Duhart P, McDonough M, Muñoz J, Martin M, Villeneuve M (2001) El complejo metamórfico Bahía Mansa en la Cordillera Costa del centro-sur de Chile (39°30′–42°00′S): geocronología K–Ar, 40Ar/39Ar y U–Pb: implicancias en la evolución del margen sur-occidental de Gondwana. Rev Geol Chil 28:179–208

Dungan MA, Wulff A, Thompson R (2001) Eruptive stratigraphy of the Tatara-San Pedro complex, 36°S, southern volcanic zone Chilean Andes: reconstruction method and implications for magma evolution at long-lived arc volcanic centers. J Petrol 42:555–626. doi:10.1093/petrology/42.3.555

Dulski P (2001) Reference materials for geochemical studies: new analytical data by ICP-MS and critical discussion of reference values. Geostand Newsl 25:87–125. doi:10.1111/j.1751-908X.2001.tb00790.x

Feeley TC, Dungan MA, Frey FA (1998) Geochemical constraints on the origin of mafic and silicic magmas at Cordón El Guadal, Tatara-San Pedro Complex, central Chile. Contrib Miner Petrol 131:394–411. doi:10.1007/s004100050400

Ferraris P (1981) Hoja Los Angeles-Angol, mapas geológicos preliminaries de Chile, escala 1:250000. Instituto de Investigaciones Geológicas de Chile (inédito), Santiago de Chile, Chile, p 56

França AB, Milani EJ, Schneider RL, López P, López MJ, Suárez S, Santa Ana H, Wiens F, Ferreiro O, Rossello EA, Bianucci HA, Flores RFA, Vistalli MC, Fernández-Seveso F, Fuenzalida RP, Muñoz N (1995) Phanerozoic correlation in Southern South America. In: Tankard AJ, Suárez Soruco R, Welsink HJ (Eds) Petroleum basins of South America. AAPG Memoir 62, pp 129–161

Ferguson KM, Dungan MA, Davidson JP, Colucci MT (1992) The Tatara-San Pedro volcano 36°S, Chile: a chemically variable dominantly mafic magmatic system. J Petrol 33:1–43

Frey FA, Gerlach DC, Hickey RL, López-Escobar L, Munizaga-Villavicencio F (1984) Petrogenesis of the Laguna De Maule volcanic complex, Chile 36°S. Contrib Miner Petrol 88:133–149. doi:10.1007/BF00371418

Gerlach DC, Frey FA, Moreno-Roa H, López-Escobar L (1988) Recent volcanism in the Puyehue—Cordon Caulle region, Southern Andes, Chile 40.5°S: petrogenesis of evolved lavas. J Petrol 29:333–382

Glodny J, Lohrmann J, Echtler H, Gräfe K, Seifert W, Collao S, Figueroa O (2005) Internal dynamics of a paleoaccretionary wedge: insights from combined isotope tectonochronology and sandbox modeling of the South-Central Chilean forearc. Earth Planet Sci Lett 231:23–39. doi:10.1016/j.epsl.2004.12.014

Glodny J, Echtler H, Figueroa O, Franz G, Gräfe K, Kemnitz H, Kramer W, Krawczyk C, Lohrmann J, Lucassen F, Melnick D, Rosenau M, Seifert W (2006) Long-term geological evolution and mass flow balance of the South-Central Andes. In: Oncken O, Chong G, Franz G, Giese P, Götze H-J, Ramos VA, Strecker MR, Wigger P (eds) The Andes—active subduction orogeny. Frontiers in Earth Science Series, vol 1. Springer, Berlin, pp 401–428

Glodny J, Gräfe K, Echtler H, Rosenau M (2008) Mesozoic to Quaternary continental margin dynamics in South-Central Chile (36–42°S): the apatite and zircon fission track perspective. Int J Earth Sci 97:1271–1291. Geol Rundsch. doi:10.1007/s00531-007-0203-1

González Bonorino G (1991) Late Paleozoic orogeny in the north-western Gondwana continental margin, western Argentina and Chile. J S Am Earth Sci 4:131–144. doi:10.1016/0895-9811(91)90023-E

Grunder AL, Mahood GA (1988) Physical and chemical models of zoned silicic magmas: the Loma Seca tuff and Calabazos caldera, Southern Andes. J Petrol 29:831–867

Hervé F (1988) Late Paleozoic subduction and accretion in southern Chile. Episodes 11:183–188

Hervé F, Munizaga F, Parada MA, Brook M, Pankhurst RJ, Snelling NJ, Drake R (1988) Granitoids of the Coast Range of central Chile: geochronology and geologic setting. J S Am Earth Sci 1:185–194. doi:10.1016/0895-9811(88)90036-3

Hickey RL, Gerlach DC, Frey FA (1984) Geochemical variations in volcanic rocks from central-south Chile. In: Harmon RS, Barreiro B (eds) Andean magmatism: chemical and isotopic constraints. Shiva, Cheshire, pp 72–95

Hickey RL, Frey FA, Gerlach DC, López-Escobar L (1986) Multiple sources for basaltic arc rocks from the Southern Volcanic Zone of the Andes (34°–41°S): trace element and isotope evidence for contributions from subducted oceanic crust, mantle, and continental crust. J Geophys Res B91:5963–5983. doi:10.1029/JB091iB06p05963

Hickey-Vargas R, Moreno-Roa H, López-Escobar L, Frey FA (1989) Geochemical variations in Andean basaltic and silicic magmas from the Villarica-Lanin volcanic chain (39.5°S): an evaluation of source heterogeneity, fractional crystallization, and crustal assimilation. Contrib Miner Petrol 103:361–386. doi:10.1007/BF00402922

Hildreth W, Moorbath S (1988) Crustal contribution to arc magmatism in the Andes of Central Chile. Contrib Miner Petrol 98:455–489. doi:10.1007/BF00372365

Jicha BR, Singer BS, Beard BL, Johnson CM, Moreno-Roa H, Naranjo JA (2007) Rapid magma ascent and generation of ^{230}Th excesses in the lower crust at Puyehue-Cordón Caulle southern volcanic zone Chile. Earth Planet Sci Lett 255:229–242. doi:10.1016/j.epsl.2006.12.017

Kay SM, Godoy E, Kurtz A (2005) Episodic arc migration, crustal thickening, subduction erosion, and magmatism in the south-central Andes. GSA Bull 117:67–88

Kilian R, Behrmann JH (2003) Geochemical constraints on the sources of Southern Chile trench sediments and their recycling in arc magmas of the Southern Andes. J Geol Soc Lond 160:57–70. doi:10.1144/0016-764901-143

Kukowski N, Oncken O (2006) Subduction erosion—the 'normal' mode of fore-arc material transfer along the Chilean margin? In: Oncken O, Chong G, Franz G, Giese P, Götze H-J, Ramos VA, Strecker MR, Wigger P (eds) The Andes—active subduction orogeny. Frontiers in Earth Science Series, vol 1. Springer, Berlin, pp 217–236

Lamy F, Hebbeln D, Röhl U, Wefer G (2001) Holocene rainfall variability in Southern Chile: a marine record of latitudinal shifts of Southern westerlies. Earth Planet Sci Lett 185:369–382. doi:10.1016/S0012-821X(00)00381-2

Lara LE, Rodriguez C, Moreno H, Perez De Arce C (2001) K–Ar geochronology and geochemistry of the upper Pliocene–Pleistocene volcanism of the southern Andes (39–42°S). Rev Geol Chil 28:67–90

Lindquist KG, Engle K, Stahlke D, Price E (2004) Global topography and bathymetry grid improves research efforts. Eos Trans AGU 85:186

Lohrmann J, Kukowski N, Krawczyk CM, Oncken O, Sick C, Sobiesiak M, Rietbrock A (2006) Subduction channel evolution in brittle forearc wedges—a combined study with scaled sandbox experiments, seismological and reflection seismic data and geological field evidence. In: Oncken O, Chong G, Franz G, Giese P, Götze H-J, Ramos VA, Strecker MR, Wigger P (eds) The Andes—active subduction orogeny. Frontiers in Earth Science Series, vol 1. Springer, Berlin, pp 237–262

López-Escobar L (1984) Petrology and chemistry of volcanic rocks of the southern Andes. In: Harmon RS, Barreiro B (eds) Andean magmatism: chemical and isotopic constraints. Shiva, Cheshire, pp 47–71

López-Escobar L, Vergara MM (1997) Eocene–Miocene longitudinal depression and quaternary volcanism in the southern Andes, Chile (33–42.5°S): a geochemical comparison. Rev Geol Chil 24:227–244

López-Escobar L, Vergara MM, Frey FA (1981) Petrology and geochemistry of lavas from Antuco volcano—a basaltic volcano of the southern Andes (37°25′). J Volcanol Geotherm Res 11:329–352. doi:10.1016/0377-0273(81)90030-5

López-Escobar L, Parada MA, Moreno H, Frey FA, Hickey-Vargas R (1992) A contribution to the petrogenesis of Osorno and Calbuco volcanoes southern Andes (41°00′–41°30′): comparative study. Rev Geol Chil 19:211–226

López-Escobar L, Parada MA, Hickey-Vargas R, Frey FA, Kempton PD, Moreno-Roa H (1995) Calbuco volcano and minor eruptive centers distributed along the Liquiñe-Ofqui fault zone Chile (41°–42°S): contrasting origin of andesitic and basaltic magma in the southern volcanic zone of the Andes. Contrib Mineral Petrol 119:345–361. doi:10.1007/BF00286934

López-Gamundi OR, Rossello EA (1998) Basin fill evolution and paleotectonic patterns along the Samfrau geosyncline: the Sauce Grande basin—Ventana fold belt (Argentina) and Karoo basin-Cape foldbelt (South Africa) revisited. Geol Rundsch 86:819–834. doi:10.1007/s005310050179

Lucassen F, Franz G, Thirlwall MF, Mezger K (1999) Crustal recycling of metamorphic basement: Late Paleozoic granites of the Chilean Coast Range and Precordillera at 22°S. J Petrol 40:1527–1551. doi:10.1093/petrology/40.10.1527

Lucassen F, Trumbull R, Franz G, Creixell C, Vasquez P, Romer RL, Figueroa O (2004) Distinguishing crustal recycling and juvenile additions at active continental margins: the Paleozoic to Recent compositional evolution of the Chilean Pacific margin (36–41°S). J S Am Earth Sci 17:103–119. doi:10.1016/j.jsames.2004.04.002

Martin MW, Kato TT, Rodríguez C, Godoy E, Duhart P, McDonough M, Campos A (1999) Evolution of the late Paleozoic accretionary complex and overlying forearc–magmatic arc, south central Chile (38°–41°S): constraints for the tectonic setting along the southwestern margin of Gondwana. Tectonics 18:582–605. doi:10.1029/1999TC900021

McDonough WF, Sun S-S (1995) Composition of the Earth. Chem Geol 120:223–253. doi:10.1016/0009-2541(94)00140-4

McLennan SM, Taylor SR, McCulloch MT, Maynard JB (1990) Geochemical and Nd–Sr isotopic composition of deep-sea turbidites: crustal evolution and plate tectonic associations. Geochim Cosmochim Acta 54:2015–2050. doi:10.1016/0016-7037(90)90269-Q

Melnick D, Echtler H (2006) Inversion of forearc basins in south central Chile caused by rapid glacial age trench fill. Geology 34:709–712. doi:10.1130/G22440.1

Mix AC, Tiedemann R, Blum P, The Shipboard Scientists (2003) Proceedings of the Ocean Drilling Program, Initial Reports, vol 202

Muñoz JB, Stern CR (1988) The Quaternary volcanic belt of the southern continental margin of South America: traverse structural and petrochemical variations across the segment 38°–39°S. J S Am Earth Sci 1:147–161. doi:10.1016/0895-9811(88)90032-6

Muñoz J, Troncoso R, Duhart P, Crignola P, Farmer L, Stern CR (2000) The relation of the mid-Tertiary coastal magmatic belt in south-central Chile to the late Oligocene increase in plate convergence rate. Rev Geol Chil 27:177–203

Nesbitt HW, Young GM (1982) Early Proterozoic climates and plate motions inferred from major element chemistry of lutites. Nature 299:715–717

Nesbitt HW, Young GM (1984) Prediction of some weathering trends of plutonic and volcanic rocks based on thermodynamic and kinetic considerations. Geochim Cosmochim Acta 48:1523–1534. doi:10.1016/0016-7037(84)90408-3

Notsu K, López-Escobar L, Onuma N (1987) Along-arc variation of Sr-isotope composition in volcanic rocks from the southern Andes (33°–55°S). Geochem J 21:307–313

Pankhurst RJ, Weaver SD, Hervé F, Larrondo P (1999) Mesozoic–Cenozoic evolution of the North Patagonian Batholith in Aysén, southern Chile. J Geol Soc 156:673–694. doi:10.1144/gsjgs.156.4.0673

Plank T, Langmuir CH (1998) The geochemical composition of subducting sediment and its consequences for the crust and mantle. Chem Geol 145:325–394. doi:10.1016/S0009-2541(97)00150-2

Raitzsch M, Völker D, Heubeck C (2007) Neogene sedimentary and mass-wasting processes on the continental margin off south-central Chile inferred from dredge samples. Mar Geol 244:166–183. doi:10.1016/j.margeo.2007.06.007

Reichert C, Schreckenberger B (2002) Cruise Report SO-161, Legs 2 and 3, SPOC. p 142

SERNAGEOMIN (2003) Mapa Geológico de Chile: versión digital. Servicio Nacional de Geología y Minería, Publicación Geológica Digital, No. 4 (edición 2003), Santiago de Chile

Shreve LR, Cloos M (1986) Dynamics of sediment subduction, melange formation, and prism accretion. J Geophys Res 91:10229–10245. doi:10.1029/JB091iB10p10229

Sigmarsson O, Chmele J, Morris J, Lopez-Escobar L (2002) Origin of ^{226}Ra–^{230}Th disequilibria in arc lavas from southern Chile and implications for magma transfer time. Earth Planet Sci Lett 196:189–196. doi:10.1016/S0012-821X(01)00611-2

Somoza R (1998) Updated Nazca (Farallon)-South America relative motions during the last 40 My: implications for mountain building in the Central Andean region. J S Am Earth Sci 11:211–215. doi:10.1016/S0895-9811(98)00012-1

Sun SS, McDonough WF (1989) Chemical and isotopic systematics of oceanic basalts: implications for mantle composition and processes. In: Saunders AD, Norry MJ (eds) Magmatism in ocean basins. Geol Soc Lond Spec Publ 42: 312–345

Tebbens SF, Cande S (1997) Southeast Pacific tectonic evolution from Early Oligocene to Present. J Geophys Res 102:12035–12059. doi:10.1029/96JB02581

Thomson SN (2002) Late Cenozoic geomorphic and tectonic evolution of the Patagonian Andes between latitudes 42° and 46°S: an appraisal based on fission-track results from the transpressional intra-arc Liquiñe-Ofqui fault zone. Geol Soc Am Bull 114:1159–1173

Thornburg TM, Kulm LD (1987) Sedimentation in the Chile Trench: depositional morphologies, lithofacies, and stratigraphy. Geol Soc Am Bull 98:33–52. doi:10.1130/0016-7606(1987)98<33:SITCTD>2.0.CO;2

Tormey DR, Frey FA, López-Escobar L (1995) Geochemistry of the active Azufre–Planchon–Peteroa volcanic complex, Chile (31°15′S): evidence for multiple sources and processes in a Cordilleran arc magmatic system. J Petrol 36:265–298

Varela R, Teixeira W, Cingolani C, Dalla Salda L (1994) Edad rubidio-estroncio de granitoids de Aluminé—Rahue, Cordillera Norpatagonica, Neuquén, Argentina. 7. Congreso Geológico Chileno, Concpeción. Actas II:1254–1258

Völker D, Wiedicke M, Ladage S, Gaedicke C, Reichert C, Rauch K, Kramer W, Heubeck C (2006) Latitudinal variation in sedimentary processes in the Peru–Chile Trench off Central Chile. In: Oncken O, Chong G, Franz G, Giese P, Götze H-J, Ramos VA, Strecker MR, Wigger P (eds) The Andes—active subduction orogeny. Frontiers in Earth Science Series, vol 1. Springer, Berlin, pp 193–216

Völker D, Reichel T, Wiedicke M, Heubeck C (2008) Turbidites deposited on Southern Central Chilean seamounts: evidence for energetic turbidity currents. Mar Geol 251:15–31. doi:10.1016/j.margeo.2008.01.008

Wiedicke M et al (2002) Cruise Report SO161-5, SPOC. p 210, BGR-Nr 11241/02

Willner A, Hervé F, Massonne H-J (2000) Mineral chemistry and pressure–temperature evolution of two contrasting high-pressure low-temperature belts in the Chonos archipelago, Southern Chile. J Petrol 41:309–330. doi:10.1093/petrology/41.3.309

Willner AP, Glodny J, Gerya TV, Godoy E, Massonne H-J (2004) A counterclockwise PTt-path of high pressure–low temperature rocks from the Coastal Cordillera accretionary complex of South Central Chile: constraints for the earliest stage of subduction mass flow. Lithos 75:283–310. doi:10.1016/j.lithos.2004.03.002